



# Joint PVL Detection and Manual Ability Classification Using Semi-supervised Multi-task Learning

Jingyun Yang<sup>1</sup>, Jie Hu<sup>2</sup>, Yicong Li<sup>1</sup>, Heng Liu<sup>2</sup>, and Yang Li<sup>1</sup>(✉)

<sup>1</sup> Tsinghua-Berkeley Shenzhen Institute, Tsinghua University, Shenzhen, China  
yangli@sz.tsinghua.edu.cn

<sup>2</sup> Department of Radiology, Affiliated Hospital of Zunyi Medical University, Guizhou, China

**Abstract.** Among symptoms of cerebral palsy (CP), the degree of hand function impairment in young children is hard to assess due to large inter-personal variability and differences in evaluators' experience. To help design better treatment strategies, accurate identification and delineation of manual ability injury level is a major clinical concern. Periventricular leukomalacia (PVL), a form of brain lesion in periventricular white matter in premature infants, is a leading cause of CP and have clinical associations with motor function injuries. In this paper, we exploit the correlation between PVL lesion segmentation and manual ability classification (MAC) to improve the identification performance of both tasks for T2 FLAIR MRI scans. Particularly, we propose a semi-supervised multi-task learning framework to jointly learn from heterogeneous datasets. Two clinically related auxiliary tasks, lesion localization and ventricle segmentation, are also incorporated to improve the classification accuracy while requiring only a small amount of manual annotations. Using two datasets containing 24 labeled PVL samples and 87 labeled MAC samples, the proposed model significantly outperforms single-task methods, achieving a dice score of 0.607 for PVL lesion segmentation and 84.3% accuracy for manual ability classification.

**Keywords:** Heterogeneous multi-task learning · Semi-supervised learning · PVL lesion segmentation · Manual ability classification · Computer-aided diagnosis

## 1 Introduction

Cerebral palsy (CP) is a non-progressive interference to the developing brain, causing a range of motor function disorder among young children [11]. Among various CP symptoms, hand function impairment have large inter-personal variations and would adversely affect patients' self-care ability in their daily life [16, 21]. To help develop better treatment strategy, accurate identification and delineation of injury level in early childhood is a major clinical concern [21]. Several examination scales,

such as the Manual Ability Classification System (MACS) and the Assisting Hand Assessment (AHA) have been frequently used to assess the degree of hand function impairment in children with CP [1]. However, an individual’s performance may vary across different scales and the accuracy of assessment relies on the experience of the evaluator [15]. Furthermore, it is difficult to perform detailed assessments during infancy due to incomplete development.

Recent clinical studies have attempted to use MRI, a more objective and quantitative measurement tool to reflect motor function. For instance, [20] uses diffusion weighted MRI to explore the correlation between damaged white matter pathways and specific motor functions such as upper limbs functions. Contrary to clinical observations, the reported correlations were mostly low to moderate. On the other hand, periventricular leukomalacia (PVL), a form of ischemic brain white matter injury in premature infants have been shown to be frequently associated with motor function disorder in children with CP [9, 12]. Hence we aim to utilize the relationship between PVL and manual ability in children with CP to improve the identification of PVL and the classification of manual ability level based on T2-Weighted MRI data.

Previous works on brain MRI lesion segmentation generally focused on extracting handcrafted image features, including modal intensities, tissue probabilities, multi-scale annular filter for blobness detection [10] or patient features like age and gender for computer-aided disease diagnosis [19]. Research that focus on PVL segmentation and manual ability classification, however, seem rare except for [25], which only uses handcrafted features that is hard to generalize to new datasets. Recently, deep learning based methods that can automatically learn informative features are extensively used to tackle certain brain MRI lesion segmentation tasks [27]. *Multi-task learning*, a learning paradigm that trains two or more related tasks with shared parameters or features, is a common approach for automatically incorporating auxiliary information in neural networks. Several studies have adopted multi-task learning for MRI image processing tasks [3–5]. However, most of the deep learning methods rely on having large amounts of annotated training data, which is not a practical solution due to the high cost obtaining expert annotations.

To solve the aforementioned challenges, we propose a semi-supervised multi-task framework for jointly segmenting the PVL lesions and classifying manual ability in a small data setting, as shown in Fig. 1. In addition to the two target tasks, we consider two medically related auxiliary tasks to help improve the performance of target tasks: *lesion localization* (LL) and *ventricle segmentation* (VS). The former identifies the coordinate of each lesion center, as clinical evidence shows that PVL lesions are always detected regularly in specific locations like the thalamus and basal ganglia. The latter is also related to PVL as the volume of the ventricles changes due to white matter injuries. One advantage of this framework is that it only requires the data for each task to be partially labeled. Information learned from known labels will propagate to unlabeled data during training by using pseudo-labeling. We show in the experiment that, having only 10 out of 80 samples with ventricle annotations is sufficient to improve the target task performance.

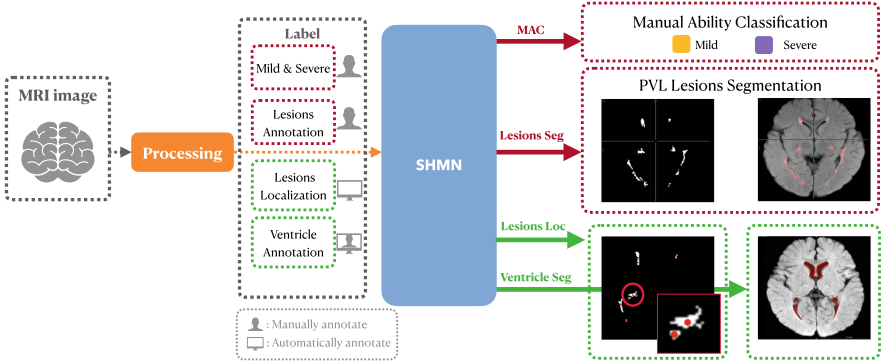


**Fig. 1.** Illustration of SHMN framework. Tasks outlined in red are the target tasks, those in green are the auxiliary tasks. (Color figure online)

The main contributions of this work are as follows:

1. We show that PVL lesions on MRI images does correlate with the manual ability level of CP patients.
2. We propose a novel deep learning framework, named Semi-supervised Heterogeneous Multi-task Network (SHMN), that can jointly learn to perform heterogeneous medical imaging tasks including segmentation, localization and classification. It effectively uses the correlation among PVL lesion condition, ventricle shape and MA level to improve the performance of manual ability classification and PVL segmentation based on MRI data.
3. We adopted an effective semi-supervised algorithm that utilizes unlabeled data in auxiliary tasks to reduce dependency on manually annotated data.

## 2 Materials and Method

### 2.1 Data and Preprocessing

Two private datasets are used in our research. **Dataset1** contains 24 T2 FLAIR MRI images with PVL lesion annotation and **Dataset2** contains 87 T2 FLAIR MRI scans with manual ability labels. For all MRI data, participants were identified through a medical record management system of the First Affiliated Hospital of Xi'an Jiaotong University. Brain images were captured using GE SignaHDxt 3.0T magnetic resonance scanner (GE Healthcare, Milwaukee, Wisconsin, USA) and 8-channel head coil.

**Dataset1** is captured from PVL patients between 19 to 28 months. Although PVL mostly occurs in newborns, premature infants younger than 1 year old often cannot tolerate MRI examinations, therefore we use MRI images of infants between 1–2 years old who are still in the relatively early stage of PVL. **Dataset2** is captured from CP patients with MA tests between 1–12 years old. These children are older since CP is commonly developed from PVL and can only be

diagnosed when children are old enough to perform certain physical tasks. Our study uses joint training to learn a better model that predicts MA level based on MRI images, which is a novel design.

PVL was characterized by white matter hyperintensities with/without tissue reduction in periventricular and was manually delineated on each slice of the patient's T2-FLAIR images by a trained rater (HJ) and reviewed by an experienced pediatric neuroradiologist (LH). ITK-SNAP [26], a software that allows simultaneous view of the brain on axial, coronal, and sagittal planes was used for manual segmentation.

Manual ability was classified using the Manual Ability Classification System (MACS). MACS is an international system to classify a child's ability of handling objects in daily activities [8]. MACS measures five levels of the manual abilities of children with CP. Level I indicates the best while level V indicates the worst level of manual ability. The specific assessment steps were described as the prior protocol [18]. All the participants were classified into two groups according to MACS levels, level I–II as mild injury group and level III–V as severe injury group.

We automatically create labels for Lesion Localization as follows: extract the topological structure of the lesion shape from the binary segmentation mask by outermost border following [23] and compute the center of mass using spatial moments.

All MRI images used in experiments are preprocessed via a standard pipeline: (i) Images are transformed into the same coordinate system by FSL FLIRT [22]. (ii) Skull stripping is performed to remove the redundant parts. (iii) Bias field correction is conducted using ANTs [2].

## 2.2 Network Architecture

Since medical images commonly encompass three dimensions, we choose 3D U-Net [6] for as our base model. The framework resides on a modified version of U-Net [14], which deviates from the original architecture in that it replaces ReLU activation functions with leaky ReLUs and uses instance normalization [24] instead of the more popular batch normalization [13]. Figure 2 shows the architecture of the proposed SHMN model which jointly learns a common encoder for all target and auxiliary tasks. The correlation among these tasks enables us to assume that their discriminative features lie in a common multi-scale feature space, represented by the encoder network. The model takes input data through one common encoder and then branch out to perform different tasks through corresponding decoders. Meanwhile, our data-driven framework incorporates semi-supervision into the learning procedures to make it few-shot friendly and reduce cost of expert annotation.

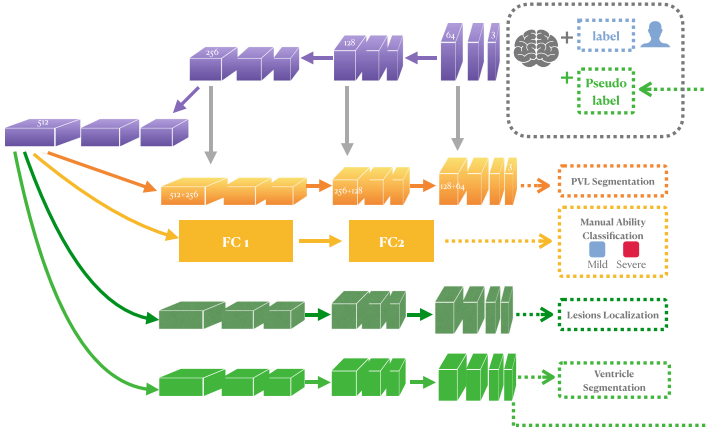


**Fig. 2.** Architecture of the multi-task semi-supervised model. The purple blocks represent the shared backbone for extracting features, and the orange and green branches are the task-specific decoders for the target tasks and auxiliary tasks, respectively. (Color figure online)

As shown in Fig. 2, the input of the network contains  $182 \times 218 \times 182$  MRI image patches with  $M_{cls}$  label (class of manual ability),  $P_{seg}$  label (PVL lesions annotation),  $L_{loc}$  label (density map) and  $V_{seg}$  label (ventricle annotation) while the target output includes the classification of manual ability and segmentation mask of PVL lesions. The common encoder uses two plain convolutional layers between pooling in each block to extract the latent features from the given images and down-samples the resolution by using the pooling technique and the respective branches receive the feature maps from the bottom. In the  $M_{cls}$  branch there is a sequence of two fully connected (FC) layers. We take the feature maps as the input of the FC1 followed by a rectified linear unit (ReLU) activation function and the output of FC1 as the input of the FC2 followed by a sigmoid activation function to predict the class probability. When the probability is greater than 0.5, we classify the sample into severe injury group. For other branches, decoders take transposed convolution operations and recombines the semantic information with higher resolution feature maps obtained directly from the encoder through skip connections. As  $V_{seg}$  aims to make full use of those unlabeled MRI data, which can be acquired easily in practice, we therefore modify the regular decoder to predict the pseudo-label for each unlabeled sample in the fine-tuning phases [17]. Due to the large image size and memory constraints we set a batch size of 2. We use the Adam optimizer with an initial learning rate of  $3e-4$  and set it to decrease periodically if the losses do not improve enough. The network is trained in a semi-supervised fashion with labeled and unlabeled data simultaneously. For unlabeled samples, pseudo-Labels recalculated after every weights update are used for the modified loss function of supervised learning task. The training procedure can be mathematically described as follows:

Let  $\mathcal{X}^1 = \{\mathbf{X}_n^1\}_{n=1}^{N_1}$  denotes the training set in Dataset1 and  $\mathcal{X}^2 = \{\mathbf{X}_n^2\}_{n=1}^{N_2}$  denotes the training set in Dataset2. We define the labels of two MAC groups (mild and severe) as  $\mathbf{y}^{mcls} = \{y_n^{mcls}\}_{n=1}^{N_1}$ , PVL lesion segmentation as  $\mathbf{y}^{pseg} = \{y_n^{pseg}\}_{n=1}^{N_2}$ , PVL lesion localization as  $\mathbf{y}^{ploc} = \{y_n^{ploc}\}_{n=1}^{N_2}$ , and ventricle segmentation as  $\mathbf{y}^{vseg} = \{y_n^{vseg}\}_{n=1}^{N_1}$ . During training, coefficients of all tasks are equally set to 1 as our work mainly focuses on the multi-task framework, however we'll explore the coefficients of different tasks in future work.

$$L_{SHMN} = \lambda_{mcls} L_{mcls} + \lambda_{pseg} L_{pseg} + \lambda_{ploc} L_{ploc} + \lambda_{vseg} L_{vseg} \quad (1)$$

Specifically, task  $M_{cls}$  is trained with the cross-entropy loss as follows:

$$L_{mcls} = -[y_{mcls} \log(\hat{y}_{mcls}) + \varepsilon(1 - y_{mcls}) \log(1 - \hat{y}_{mcls})] \quad (2)$$

where  $\varepsilon$  is the bias of positive examples to negative examples, which can increase the penalty for misclassification of positive examples.

Task  $P_{seg}$  is trained with a combination of dice and cross-entropy loss,  $L_{pseg} = L_{CE} + L_{dice}$ . The dice loss function here is an adaptation of the variant proposed in [7]:

$$L_{dice} = -2 \frac{\sum_{i \in I} o_i v_i}{\sum_{i \in I} u_i + \sum_{i \in I} v_i} \quad (3)$$

where  $o$  is the softmax output of the network and  $v$  is a one hot encoding of the ground truth segmentation map  $y_{pseg}$  and  $i \in I$  is the number of pixels in the training batch.

As for task  $V_{seg}$ , in order to provide pseudo-labels for unlabeled samples, we select the class with maximum predicted probability for each unlabeled sample.

$$y_{vseg}^{c'} = \begin{cases} 1 & \text{if } c = \operatorname{argmax}_{c'} \hat{y}_{vseg}^{c'} \\ 0 & \text{otherwise} \end{cases} \quad (4)$$

and we can add the pseudo-label to the unlabeled data and update our dataset to train with the loss function:

$$L_{vseg}^* = \alpha(t) \sum_{c=1}^C L_{vseg} \left( y_{vseg}^{c'}, \hat{y}_{vseg}^c \right) \quad (5)$$

where  $\alpha(t)$  is a coefficient balancing labeled data and pseudo-labeled data to maximize benefit of the unlabeled data.

$$\alpha(t) = \begin{cases} 0, & t < T_1; \\ \frac{t-T_1}{T_2-T_1} \alpha_f, & T_1 \leq t < T_2; \\ \alpha_f, & T_2 \leq t. \end{cases} \quad (6)$$

Task  $V_{seg}$  is trained with standard binary cross-entropy loss while task  $P_{loc}$  is trained with MSE loss for its simplicity and effectiveness.

### 3 Experiments and Results

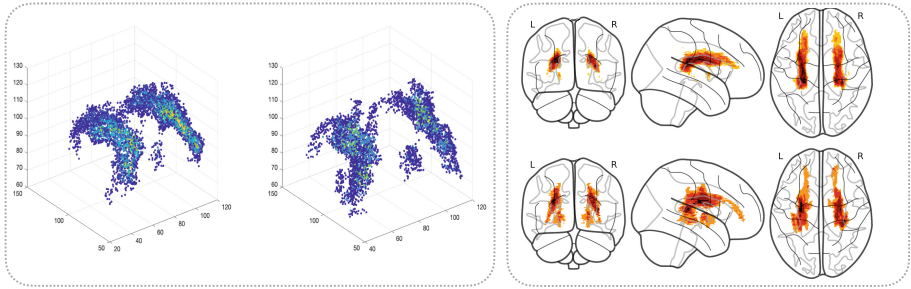


**Fig. 3.** Lesions distribution of mild (left) and severe (right) MA groups on the left and distributions of total lesion volume in mild (above) and severe (below) MA groups on the right.

First, we present the empirical evidence of the correlation between PVL lesions and MAC levels. In Fig. 3, we visualize the PVL lesion distributions in the mild injury group and the severe injury group based on 16 lesions labeled samples annotated by expert from Dataset2. Compared with the mild group, the distribution map of the CP patients with severe impairment demonstrates that the occurrence of injure follows a characteristic spatial pattern with more predilection for thalamus, basal ganglia and regions around the central sulcus which are indeed related to manual ability. The result is consistent with the clinical research.

Model training is done on two datasets containing 24 images with PVL segmentation mask and 87 images with manual ability classification 68 mild, 29 severe respectively. We divide both dataset1 and dataset2 into 70% training, 10% validation and 20% testing for two target tasks. For auxiliary tasks, Lesion Localization is trained on Dataset1 and Ventricle Segmentation is trained on Dataset2, both with a 9:1 training-validation split. The performance of manual ability classification is evaluated by accuracy and F1 score while the performance of PVL lesion segmentation is evaluated by dice. To further show the validity of the task setting, we train with different combinations of tasks via SHMN. The setting includes (1) joint MAC and PVL Lesion Segmentation (SHMN-2), (2) joint MAC and PVL Lesion Segmentation with Lesion Localization (SHMN-3), (3) joint MAC and PVL Lesion segmentation with Lesion Localization and Ventricle Segmentation (SHMN-4), (4) joint MAC and PVL Lesion Segmentation with Lesion Localization and Ventricle Segmentation using less labeled data (SHMN-4\*). Specifically we use 25 ventricle labeled MRI data in SHMN-4 while pseudo-labeling 70 more ventricle unlabeled data with only 10 labeled data in SHMN-4\*.

**Table 1.** Results of manual ability classification and PVL lesion segmentation

Method	MAC		Lesion segmentation
	Accuracy	F1	Dice
U-Net set single task	0.627	0.513	0.441
SHMN-2	0.667	0.583	0.532
SHMN-3	0.745	0.649	0.583
SHMN-4	<b>0.843</b>	<b>0.789</b>	<b>0.607</b>
SHMN-4*	0.824	0.757	0.600

As shown in Table 1, the proposed methods yield better results in both MAC and lesion segmentation compared to the conventional approach of single-task training with 3D U-Net [6]. The standard errors of MAC and of PVL segmentation are  $1.2e-3$  and  $1.6458e-2$  respectively in the SHMN-4 setting. This experiment implies that our heterogeneous multi-task model is superior to models which learn from different tasks separately. Note that every auxiliary task does help improving target task performance, proving that these medically related tasks can indeed assist in the diagnosis. Specifically, even we just use 10 ventricle labeled data in SHMN-4\*, the model can still achieve quite satisfying results. Thus we can achieve high segmentation and classification accuracy under the condition of few annotation cost.

We have also compared our model with a SOTA multi-task learning architecture [3] by augmenting the 2D U-Net baseline model with an image classification subnet. The final loss is a combination of categorical cross-entropy for image classification, and the dice loss and cross-entropy loss for PVL segmentation. Trained with the same setting as SHMN-2, the accuracy of MAC and dice score of PVL segmentation are 0.627 and 0.531 respectively, compared to 0.667 and 0.532 for our result with SHMN-2. This demonstrates that our architecture choice for multi-task learning is more effective than the previous work.

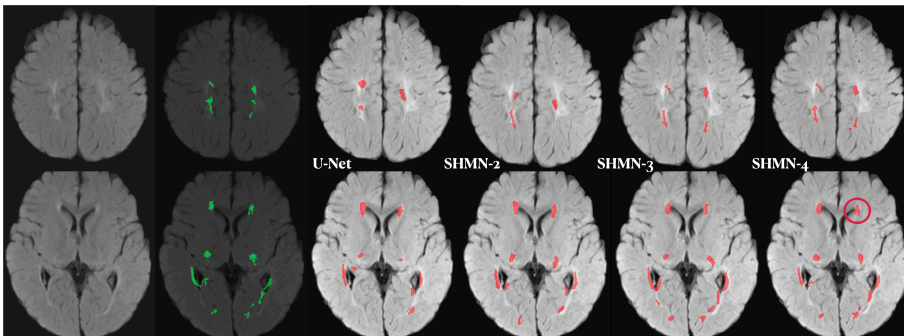


**Fig. 4.** A visual demonstration of the performance of the proposed SHMN. From left to right: sample T2 FLAIR slices; expert annotations of PVL lesions in green; segmentation of PVL lesions generated by U-Net and SHMN with different task setting in red. Two rows represent different axial slices of the same instance. (Color figure online)

Moreover, Fig. 4 demonstrates the segmentation results compared with the expert annotation for the visual assessment of SHMN. Task setting is the same as above. It is worth noting that after adding the ventricle segmentation task, the model become more ventricle-sensitive in the PVL lesions segmentation observed from the circled area.

To further evaluate SHMN’s effectiveness in the semi-supervised scenario, we train our model with 5, 10, 15 and 20 ventricle segmentation labels and show their MAC results in Fig. 5. Good classification accuracy can be achieved with as few as 10 ventricle labels using our semi-supervised model.

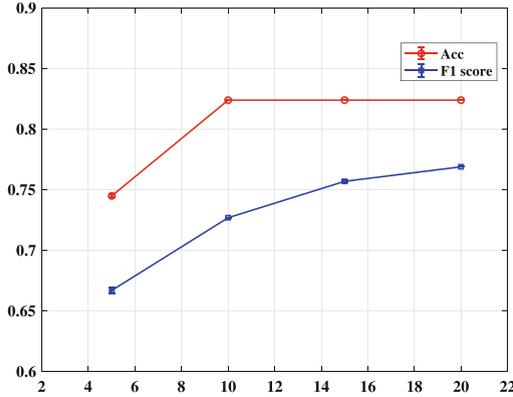


Fig. 5. Accuracy and F1 score of  $M_{cls}$  with different sizes of labeled data used in  $V_{seg}$

## 4 Discussion

In this paper an automatic and simple framework is presented for the medical domain that can precisely detect small periventricular white matter lesions and assist in the diagnosis of manual ability injury. Our work provides this novel direction that explores auxiliary tasks and make full use of them which can inspire more medical research. In our future research, we want to extend our framework with even less annotation requirements and automatic auxiliary task selection. We will consider unsupervised lesion detection by using anomaly detection and develop an algorithm that picks the most useful auxiliary tasks to train based on automatically computed task relevance.

**Acknowledgements.** This work was supported by the National Natural Science Foundation of China (Grant No. 81901732) and the Science and Technology Supporting Program of Guizhou Province (Grant No. qiankehezhiheng S[2020]2359).

## References

1. Arner, M., Eliasson, A.C., Nicklasson, S., Sommerstein, K., Hägglund, G.: Hand function in cerebral palsy. Report of 367 children in a population-based longitudinal health care program. *J. Hand Surg.* **33**(8), 1337–1347 (2008)

2. Avants, B.B., Tustison, N.J., Stauffer, M., Song, G., Wu, B., Gee, J.C.: The insight toolkit image registration framework. *Front. Neuroinform.* **8**, 44 (2014)
3. Sainz de Cea, M.V., Diedrich, K., Bakalo, R., Ness, L., Richmond, D.: Multi-task learning for detection and classification of cancer in screening mammography. In: Martel, A.L., et al. (eds.) *MICCAI 2020*. LNCS, vol. 12266, pp. 241–250. Springer, Cham (2020). [https://doi.org/10.1007/978-3-030-59725-2\\_24](https://doi.org/10.1007/978-3-030-59725-2_24)
4. Chen, C., Bai, W., Rueckert, D.: Multi-task learning for left atrial segmentation on GE-MRI. In: Pop, M., et al. (eds.) *STACOM 2018*. LNCS, vol. 11395, pp. 292–301. Springer, Cham (2019). [https://doi.org/10.1007/978-3-030-12029-0\\_32](https://doi.org/10.1007/978-3-030-12029-0_32)
5. Cheng, G., Cheng, J., Luo, M., He, L., Tian, Y., Wang, R.: Effective and efficient multitask learning for brain tumor segmentation. *J. Real-Time Image Proc.* **17**(6), 1951–1960 (2020)
6. Çiçek, Ö., Abdulkadir, A., Lienkamp, S.S., Brox, T., Ronneberger, O.: 3D U-Net: learning dense volumetric segmentation from sparse annotation. In: Ourselin, S., Joskowicz, L., Sabuncu, M.R., Unal, G., Wells, W. (eds.) *MICCAI 2016*. LNCS, vol. 9901, pp. 424–432. Springer, Cham (2016). [https://doi.org/10.1007/978-3-319-46723-8\\_49](https://doi.org/10.1007/978-3-319-46723-8_49)
7. Drozdal, M., Vorontsov, E., Chartrand, G., Kadoury, S., Pal, C.: The importance of skip connections in biomedical image segmentation. In: Carneiro, G., et al. (eds.) *LABELS/DLMIA -2016*. LNCS, vol. 10008, pp. 179–187. Springer, Cham (2016). [https://doi.org/10.1007/978-3-319-46976-8\\_19](https://doi.org/10.1007/978-3-319-46976-8_19)
8. Eliasson, A.C., et al.: The manual ability classification system (MACS) for children with cerebral palsy: scale development and evidence of validity and reliability. *Dev. Med. Child Neurol.* **48**(7), 549–554 (2006)
9. Franki, I., et al.: The relationship between neuroimaging and motor outcome in children with cerebral palsy: a systematic review-part a. Structural imaging. *Res. Dev. Disabil.* **100**, 103606 (2020)
10. Ghafoorian, M., et al.: Small white matter lesion detection in cerebral small vessel disease. In: *Medical Imaging 2015: Computer-Aided Diagnosis*, vol. 9414, p. 941411. International Society for Optics and Photonics (2015)
11. Graham, H.K., et al.: Erratum: cerebral palsy. *Nat. Rev. Dis. Primers.* **2**(1), 15082 (2016)
12. Holmefur, M., et al.: Neuroradiology can predict the development of hand function in children with unilateral cerebral palsy. *Neurorehabil. Neural Repair* **27**(1), 72–78 (2013)
13. Ioffe, S., Szegedy, C.: Batch normalization: accelerating deep network training by reducing internal covariate shift. In: *International Conference on Machine Learning*, pp. 448–456. PMLR (2015)
14. Isensee, F., et al.: nnU-Net: self-adapting framework for u-net-based medical image segmentation. *arXiv preprint arXiv:1809.10486* (2018)
15. Jiang, H., et al.: Specific white matter lesions related to motor dysfunction in spastic cerebral palsy: a meta-analysis of diffusion tensor imaging studies. *J. Child Neurol.* **35**(2), 146–154 (2020)
16. Klingels, K., et al.: Upper limb impairments and their impact on activity measures in children with unilateral cerebral palsy. *Eur. J. Paediatr. Neurol.* **16**(5), 475–484 (2012)
17. Lee, D.H., et al.: Pseudo-label: the simple and efficient semi-supervised learning method for deep neural networks. In: *Workshop on Challenges in Representation Learning, ICML*, vol. 3 (2013)

18. Liu, H., et al.: Treatment response prediction of rehabilitation program in children with cerebral palsy using radiomics strategy: protocol for a multicenter prospective cohort study in west China. *Quant. Imaging Med. Surg.* **9**(8), 1402 (2019)
19. Liu, M., Zhang, J., Adeli, E., Shen, D.: Deep multi-task multi-channel learning for joint classification and regression of brain status. In: Descoteaux, M., Maier-Hein, L., Franz, A., Jannin, P., Collins, D.L., Duchesne, S. (eds.) *MICCAI 2017. LNCS*, vol. 10435, pp. 3–11. Springer, Cham (2017). [https://doi.org/10.1007/978-3-319-66179-7\\_1](https://doi.org/10.1007/978-3-319-66179-7_1)
20. Mailleux, L., Franki, I., Emsell, L., Peedima, M.L., Fehrenbach, A., Feys, H., Ortibus, E.: The relationship between neuroimaging and motor outcome in children with cerebral palsy: a systematic review-part b diffusion imaging and tractography. *Res. Dev. Disabil.* **97**, 103569 (2020)
21. Mailleux, L., et al.: White matter characteristics of motor, sensory and interhemispheric tracts underlying impaired upper limb function in children with unilateral cerebral palsy. *Brain Struct. Funct.* **225**(5), 1495–1509 (2020)
22. Smith, S.M., et al.: Advances in functional and structural MR image analysis and implementation as FSL. *Neuroimage* **23**, S208–S219 (2004)
23. Suzuki, S., et al.: Topological structural analysis of digitized binary images by border following. *Comput. Vis. Graph. Image Process.* **30**(1), 32–46 (1985)
24. Ulyanov, D., Vedaldi, A., Lempitsky, V.: Instance normalization: the missing ingredient for fast stylization. *arXiv preprint arXiv:1607.08022* (2016)
25. Wang, J., Huang, C., Wang, Z., Zhang, Y., Ding, Y., Xiu, J.: Anchor-based segmentation of periventricular white matter for neonatal HIE. *IEEE Access* **8**, 73547–73557 (2020)
26. Yushkevich, P.A., et al.: User-guided 3D active contour segmentation of anatomical structures: significantly improved efficiency and reliability. *Neuroimage* **31**(3), 1116–1128 (2006)
27. Zeng, C., Gu, L., Liu, Z., Zhao, S.: Review of deep learning approaches for the segmentation of multiple sclerosis lesions on brain MRI. *Front. Neuroinform.* **14**, 55 (2020)